

CONSTRAINING THE CIRCUMBURST MEDIUM OF GAMMA-RAY BURSTS WITH X-RAY AFTERGLOWS

XIAO TIAN¹, YING QIN², MEI DU¹, SHUANG-XI YI¹ AND YAN-KE TANG³

¹School of Physics and Physical Engineering, Qufu Normal University, Qufu 273165, China; yisx2015@qfnu.edu.cn

²Department of Physics, Anhui Normal University, Wuhu 241000, China; yingqin2013@hotmail.com

³College of Physics and Electronic, Dezhou University, Dezhou 253023, China.

ABSTRACT

Long gamma-ray bursts (GRBs) are considered to be originated from core collapse of massive stars. It is believed that the afterglow property is determined by the density of the material in the surrounding interstellar medium. Therefore, the circumburst density can be used to distinguish between an interstellar wind $n(R) \propto R^{-k}$, and a constant density medium (ISM), $n(R) = \text{const}$. Previous studies with different afterglow samples, show that the circumburst medium of GRBs is neither simply supported by an interstellar wind, nor completely favored by an ISM. In this work, our new sample is consisted of 39 GRBs with smoothly onset bump-like features in early X-ray afterglows, in which 20 GRBs have the redshift measurements. By using a smooth broken power law function to fit the bumps of X-ray light curves, we derive the full width at half-maximum (FWHM) as the feature width (ω), as well as the rise and decay time scales of the bumps (T_r and T_d). The correlations between the timescales of X-ray bumps are similar to those found previously in the optical afterglows. Based on the fireball forward shock (FS) model of the thin shell case, we obtain the distribution of the electron spectral index p , and further constrain the medium density distribution index k . The new inferred k is found to be concentrated at 1.0, with a range from 0.2 to 1.8. This finding is consistent with previous studies. The conclusion of our detailed investigation for X-ray afterglows suggests that the ambient medium of the selected GRBs is not homogeneous, i.e., neither ISM nor the typical interstellar wind.

Keywords: Gamma-ray bursts (629); Non-thermal radiation sources (1119)

1. INTRODUCTION

Gamma-ray bursts (GRBs) are the brightest phenomena in the universe. With more observational detectors launched successfully, the understanding of the origins for GRBs is becoming more and more profound (Gehrels et al. 2004; Burrows et al. 2005; Roming et al. 2005; Atwood et al. 2009; Meegan et al. 2009; Li et al. 2020a; Zhang et al. 2020). One of the most popular model of the dominant mechanism for GRBs is the fireball model (Mészáros 2002; Zhang & Mészáros 2004; Piran 2004), by which the prompt γ -ray emission can be explained by the internal dissipative processes occurring in relativistic ejecta or due to internal shocks (Meszaros & Rees 1993; Rees & Meszaros 1994), and by which the multi-band afterglow emission is produced by the synchrotron emission of the external shock when the fireball is decelerated by the ambient medium (Mészáros & Rees 1997; Sari et al. 1998; Wang et al. 2018; Du et al. 2021).

GRBs, based on the prompt burst duration T_{90} , can be divided into two groups: long GRBs ($T_{90} > 2s$) and short GRBs ($T_{90} < 2s$) (Qin et al. 2013; Wang et al. 2020). Studies suggest that short GRBs are originated from the merger of binary compact stars, i.e., two neu-

tron stars or neutron star-black hole (Panaitescu & Kumar 2002), while long GRBs are related to core collapse of massive stars (Woosley 1993; MacFadyen & Woosley 1999). In this standard collapsar model, massive, fast rotating Wolf-Rayet (WR) stars are believed to be the progenitors of long GRBs. In order to maintain enough angular momentum, one has to consider WR stars with a compact companion in a close binary system, or at a low metallicity for a lower mass loss rate. In case of the first scenario, the angular momentum content of a WR is determined by tides and its stellar winds. In this context, whether a WR star with a compact companion in a close binary system can be spun up to form a collapsar or not, has been systematically investigated (Cantiello et al. 2007; Detmers et al. 2008; Liu et al. 2017; Qin et al. 2018; Liu et al. 2018). Alternatively, WR stars as the progenitors of long GRBs are single, massive stars, which must be born in a metal-poor environment to avoid losing a larger number of angular momentum through strong winds. The ejected matter from massive WRs through winds thus can enhance chemical enrichment of the host galaxies, which further makes the circumferential material density more complex. In the context of the second

scenario, when the fireball shell slows down in collision with the circumburst medium, two types of shock waves will be generated: reverse shock (RS) and forward shock (FS). The RS pierces into the fireball ejecta, while the FS propagates into the circumburst medium. The FS model predicts that when the fireball shell is decelerated by the circumferential environment, the afterglow light curves will show a smooth onset bump. A large number of early optical afterglows with smooth onset bumps have been collected in the *Swift* era, which are in a good agreement with the predictions by the external FS model (Sari & Piran 1999; Molinari et al. 2007; Rykoff et al. 2009; Liang et al. 2010, 2013; Yi et al. 2013; Zhao et al. 2020). Based on the external FS model, it is believed that the temporal and spectral index of the multi-band afterglows can be used to constrain the radiation mechanism and the properties of the circumburst medium (Sari et al. 1998; Li et al. 2020b).

Dai & Lu (1998), assuming that the expansion of the fireball is adiabatic and that the density in the medium varies as a power-law function of shock radius, $n \propto R^{-k}$, found that the X-ray afterglow of GRB 970616 is well fitted by assuming $k = 2$. By fitting the simultaneous spectra of X-ray, optical, and NIR afterglow data of 10 *BeppoSAX* GRBs, Starling et al. (2008) first investigated the density structure index of the circumburst medium. It was found that k is well constrained for five GRBs, in four of which the circumburst medium is interstellar wind medium, i.e., $k = 2$. The fifth source has k in the range of $0 - 1$, consistent with ISM. With the available optical and *Swift*/X-ray late-time afterglow, Schulze et al. (2011) found that 24% is in favor of the wind medium, while the rest (except for the short GRBs 051221A and 060904B) supports ISM. Then a following investigation for a subsample of GRB optical afterglow with onset bump features shows the index k is centered at 1 with a range of $0.4 - 1.4$ (Yi et al. 2013). This result further indicates that the GRBs ambient medium is neither ISM nor stellar wind environment, which is also consistent with the results of Liang et al. (2013).

Recently, Yi et al. (2020) also collected some optical afterglows with significant RS features, and inferred the k value in the range of $0 - 1.5$ under the assumption of the external RS model. Therefore, GRBs may have different type ambient medium. Interestingly, we find that some GRB X-ray afterglows show the onset deceleration feature. It is believed that the X-ray afterglows with smooth onset bumps, can be explained by the external FS model. Hence the investigation of the circumferential environment for GRBs with X-ray onset bump is needed. Furthermore, the X-ray afterglow is simpler when compared with the optical afterglow, and it can be clearly described in five different segments (Zhang et al. 2006; Nousek et al. 2006).

Following the previous works, we here continue to constrain GRBs circumburst medium with X-ray afterglows. The paper is organized as follows. We introduce the selection criteria of X-ray onset bump in Section 2. In the Section 3, we present the characteristics of X-ray bump and their correlations. The results for the application of the external FS model to our selected X-ray sample are shown in Section 4. We finally give our Discussions and Conclusions in Sections 5 and 6, respectively.

2. SAMPLE SELECTION AND LIGHT CURVE FITTING

The optical onset afterglows are considered as a good probe of testing the fireball external shock model since it is generally less polluted by the prompt emission tail or by the later emission of engine activity (Oates et al. 2009; Liang et al. 2010, 2013; Ghirlanda et al. 2012; Yi et al. 2017, 2021a,b). In general, an onset bump is made of two components, i.e., a slow rise and decay. Liang et al. (2010) found that the rise slope is less than 3, typically around 1 and 2. However, for the X-ray afterglows, some emissions from GRB central engine can appear in early time, including the erratic flares, plateaus or the GRB tail emission. The deceleration features in X-ray afterglows can be affected by those emission components, which are related to the activity from the central engine. Hence the sample of X-ray light curves with a clear deceleration onset bump signature is limited.

We first show three criteria for collecting the X-ray sample with the onset bump features: (1) a complete component of rise and decay feature in X-ray afterglows; (2) the rise slope less than 3; and (3) without the superposition of erratic flares or plateaus in the smooth bumps. Our target sample is consisted of 39 GRBs with a smooth bump feature in X-ray afterglows, collected from the official website of *Swift*¹ in the time period of July 2005 - October 2020. In order to derive the temporal parameters of X-ray afterglow onset bumps, we follow the previous work (Yi et al. 2016; Si et al. 2018) and use an empirical smooth broken power-law function (SBPL, Beuermann et al. 1999) to fit X-ray bumps,

$$F_{\text{model}}(t) = F_0 \left[\left(\frac{t}{T_p} \right)^{\alpha_1 b} + \left(\frac{t}{T_p} \right)^{\alpha_2 b} \right]^{-\frac{1}{b}}, \quad (1)$$

where α_1 and α_2 are the rise and decay indexes, respectively; $F_p = F_0 2^{-1/b}$ is the flux of peak time and b represents the peak sharpness of the light-curve components. We take 3 as a typical value of the parameter b . Some X-ray afterglows are usually combined of several power-law segments along with some X-ray flares, or steep decays. Therefore, we only fit the data around the X-ray onset bumps, without including mixed components. The fit-

¹ http://www.swift.ac.uk/xrt_curves/.

ting results of selected GRBs are showed in Figure 1, and the corresponding fitting parameters for each GRB are presented in Tables 1 and 2, respectively. The data of redshift (z), duration (T_{90}) and the photon index (Γ) are collected from the official website of *Swift* and are listed in Tables 1 and 2.

3. CHARACTERISTICS OF THE ONSET BUMP AND THEIR CORRELATIONS

The external FS model can well explain the optical afterglow with the onset characteristics, which is also shown in our currently selected X-ray sample. The rise index α_1 of most GRBs is found in the range of 0.3 – 2.6 and the central decay index α_2 is around -1.0. We adopt the full width at half-maximum (FWHM) of the fitted curve as the feature width (ω) of the bump. The rise and decay time scales (T_r and T_d) are defined at FWHM. We find that the peak time T_p and the width ω have the same range, i.e., 10^2 – 10^4 s. In addition, the decay time (T_d) is larger than the rise time (T_r).

By using the Spearman pair correlation analysis, we obtain the corresponding coefficients. In Figure 2, we present pair correlations for fitted parameters, as well as the best fitting result together with its 95% credibility in red. Interestingly, we find tight correlations among rise time, decay time, the peak time and the feature width. These correlations are given as follows:

$$\log T_d = (0.44 \pm 0.11) + (1.00 \pm 0.03) \log T_r, \quad (2)$$

$$\log T_r = (-0.10 \pm 0.07) + (0.95 \pm 0.02) \log T_p, \quad (3)$$

$$\log T_d = (0.25 \pm 0.11) + (0.98 \pm 0.03) \log T_p, \quad (4)$$

$$\log \omega = (0.38 \pm 0.10) + (0.98 \pm 0.03) \log T_p. \quad (5)$$

These pair correlations show well positive linear correlations, indicating that these X-ray bumps have a universal physical origin. We find that the results of these fitting coefficients are similar to those in Liang et al. (2010). This further indicates that the selected X-ray sample has the same onset characteristics as the optical light curves. Therefore, these X-ray bumps can also be explained by the external FS model. We also note that a wider X-ray bump (ω) tends to peak at a later time (T_p), which is consistent with the optical onset bumps.

The finding above is in line with the expectations of the external shock model, as the later deceleration time, corresponding to a smaller Lorentz factor, is equivalent to the peak time of onset bumps for the thin shell case. We then apply the theoretical FS model to these X-ray samples, and identify the type of circumburst medium in the following sections.

4. ANALYSES AND RESULTS

As discussed above, the observational properties of the selected X-ray bumps could be produced by the deceleration of a fireball shell. Therefore, we apply the external FS model to those X-ray bumps. In the standard FS model, the theoretical rise index is 3 in the regime $\nu_m^f < \nu < \nu_c^f$ (or 2 for $\nu > \max\{\nu_c^f, \nu_m^f\}$) for the ISM case, and the index is 0.5 for the interstellar wind environment. Since the rise index of most X-ray bumps is in the range of 0.3 – 2.6, it's hardly to determine the real type of the circumburst medium of those GRBs. Therefore, we assume that the general density distribution of long GRB ambient medium is $n = AR^{-k}$, where n is the density of proton number, R is the radius, and k is the density distribution index of the medium. Through previous works, we obtain the value $k = 0$ for the interstellar medium case and $k = 2$ for the interstellar wind environment, respectively.

A large number of optical afterglows have been collected since 1997, some of which show clear smooth bumps and sharp RS signatures for different optical light curves (Liang et al. 2010; Japelj et al. 2014). We successfully applied the external shock model of thin shell case to those optical afterglows with the onset bump features and signatures of dominant RS emission respectively, as well as identified the types of GRB ambient medium (Yi et al. 2013, 2020; Zhou et al. 2020). Following the previous works, we now continue to constrain the types of GRB circumburst medium with the selected X-ray onset bumps in this work. The method we adopt here is the same as that proposed before. The FS theoretical flux density of the thin shell before and after the peak time are (Yi et al. 2013; Zhou et al. 2020):

$$F_\nu^{FS}(t < T_\Delta) \propto \begin{cases} t^{\frac{8-2k-kp}{4}} \nu^{-\frac{p}{2}}, & \nu > \max\{\nu_c^f, \nu_m^f\} \\ t^{\frac{12-5k-kp}{4}} \nu^{-\frac{p-1}{2}}, & \nu_m^f < \nu < \nu_c^f \\ t^{\frac{8-3k}{4}} \nu^{-\frac{1}{2}}, & \nu_c^f < \nu < \nu_m^f \end{cases} \quad (6)$$

and

$$F_\nu^{FS}(t > T_\Delta) \propto \begin{cases} t^{-\frac{3p-2}{4}} \nu^{-\frac{p}{2}}, & \nu > \max\{\nu_c^f, \nu_m^f\} \\ t^{-\frac{12p-3kp-12+5k}{4(4-k)}} \nu^{-\frac{p-1}{2}}, & \nu_m^f < \nu < \nu_c^f \\ t^{-\frac{1}{4}} \nu^{-\frac{1}{2}}, & \nu_c^f < \nu < \nu_m^f \end{cases} \quad (7)$$

where the ν_m^f is the typical frequency, the ν_c^f is cooling frequency and T_Δ is the RS crossing time. More details can be found in Yi et al. (2013). The real conditions of GRB ambient medium may be more complex, but it should be a viable approach when considering both temporal slopes and X-ray spectral indexes for determining the types of GRB circumburst medium. Since the medium density distribution index k and electron spec-

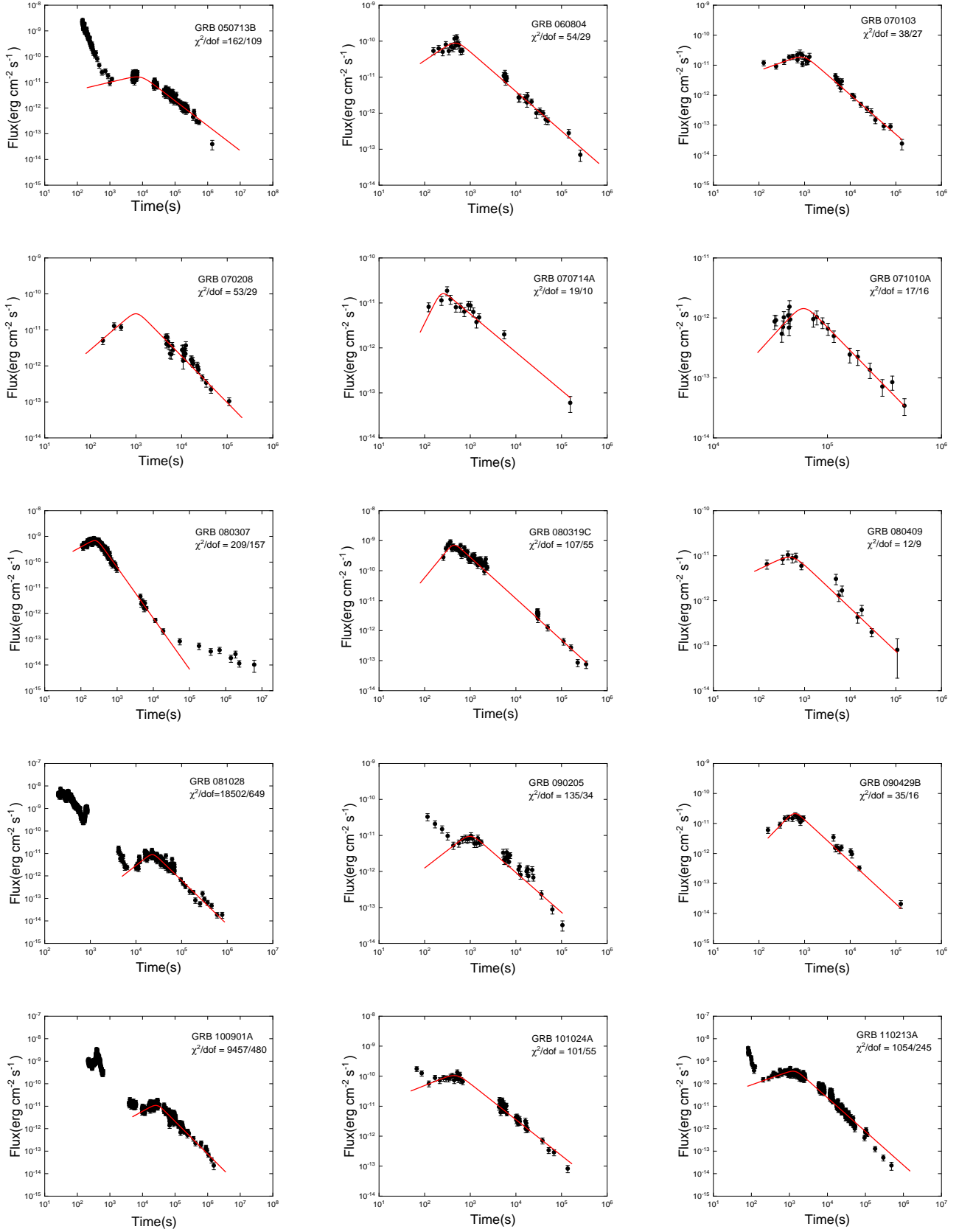


Figure 1. Light curves of the X-ray selected sample. The black dots represent the X-ray data, while the solid red lines are the fitting lines.

Table 1. Properties of the GRB Sample with Well-sampled X-ray Light Curves ($\nu > \max\{\nu_c^f, \nu_m^f\}$)

GRB	z	T_{90}^b	Γ	F_p^a	α_1	α_2	T_p^b	χ^2/dof	ω^b	T_r^b	T_d^b	k	p
050713B	...	54.2	1.94±0.12	1.55±0.09	0.30±0.09	-0.98±0.02	9090±780	162/109	22488±3766	6951±1171	15537±3745	1.71±0.09	1.97±0.03
070103	2.6208	18.6	2.10±0.27	1.81±0.17	0.55±0.16	-1.32±0.05	905±124	38/27	1673±447	610±165	1063±450	1.31±0.14	2.43±0.06
070208	1.165	48	2.05±0.19	2.81±0.47	1.09±0.25	-1.29±0.06	968±130	53/29	2013±639	608±174	1405±642	0.83±0.23	2.39±0.08
080409	...	20.2	1.99±0.39	0.90±0.14	0.50±0.34	-0.96±0.07	548±171	12/9	1303±772	349±230	953±776	1.52±0.34	1.95±0.09
100901A	1.408	439	2.11±0.06	1.13±0.03	0.80±0.07	-1.45±0.03	26437±893	9457/480	43367±3301	13101±1363	30266±3261	1.04±0.06	2.60±0.04
120118B	2.943	23.26	1.98±0.15	1.13±0.08	0.79±0.20	-0.91±0.08	1508±256	310/41	3715±1215	804±332	2911±1224	1.25±0.21	1.88±0.11
120215A	...	26.5	2.22±0.20	0.15±0.02	1.30±0.42	-0.90±0.06	11704±1601	351/45	32806±9547	5655±2221	27151±9557	0.72±0.44	1.87±0.07
120224A	1.1	8.13	2.10±0.13	2.76±0.13	0.80±0.11	-1.00±0.03	1379±121	167/80	3865±623	953±144	2911±630	1.20±0.11	2.00±0.03
121209A	2.1	42.7	2.11±0.13	15.79±1.96	0.92±0.21	-1.23±0.03	752±81	134/89	1523±390	460±115	1063±390	1.00±0.20	2.31±0.05
130807A ^c	2.40±0.50	0.27±0.03	1.60±0.68	-0.93±0.06	9067±1721	7651/190	24816±10167	4278±2361	20539±10185	0.41±0.69	1.91±0.08
140719A	...	48	2.16±0.20	0.75±0.19	0.83±0.37	-0.99±0.05	2456±673	106/35	6754±4076	1666±853	5088±4097	1.17±0.37	1.99±0.06
151112A	4.1	19.32	2.16±0.16	0.59±0.04	1.57±0.56	-1.04±0.04	5118±382	60/45	9945±1790	2448±626	7497±1762	0.42±0.55	2.05±0.05
151114A	...	4.86	2.01±0.20	2.05±0.33	0.47±0.35	-1.12±0.06	439±90	14/12	1007±432	285±148	721±426	1.47±0.34	2.16±0.08
171123A	...	58.5	2.06±0.23	0.40±0.03	0.77±0.29	-0.75±0.09	1800±463	90/23	6951±3082	1260±531	5691±3106	1.34±0.32	1.67±0.12
190422A	...	212	2.09±0.18	3.94±0.29	1.11±0.24	-0.79±0.04	2993±291	154/87	8583 ±1909	1857±377	6726±1916	0.96±0.26	1.72±0.05
190828B	...	66.6	2.03±0.11	11.09±0.56	0.91±0.17	-1.09±0.02	694±47	1898/116	1608±236	348±71	1260± 235	1.06±0.17	2.12±0.02
200409A	...	17.91	2.06±0.17	2.30±0.28	0.70±0.41	-0.89±0.03	300±60	46/29	985±383	179±85	807±383	1.35±0.42	1.85±0.04
200925B	...	18.25	2.13±0.19	2.47±0.21	0.47±0.17	-1.04±0.04	1000±167	123/27	2325±722	659±222	1666±727	1.51±0.16	2.05±0.05

NOTE—

^a F_p is the peak flux for the bump, and in units of $10^{-11} \text{ erg cm}^{-2} \text{ s}^{-1}$.^b In units of seconds.^c The T_{90} of GRB 130807A is not available, but GRB 130807A can be identified as a long burst from Swift/BAT light curve.**Table 2.** Properties of the GRB Sample with Well-sampled X-ray Light Curves ($\nu_m^f < \nu < \nu_c^f$)

GRB	z	T_{90}^b	Γ	F_p^a	α_1	α_2	T_p^b	χ^2/dof	ω^b	T_r^b	T_d^b	k	p
060804	...	17.8	1.89±0.19	8.83±0.71	0.85±0.32	-1.10±0.03	419±56	54/29	920±255	199±83	721±253	1.20±0.18	2.18±0.08
070714A	1.58	2	2.05±0.34	1.56±0.16	2.05±0.77	-0.86±0.05	234±32	19/10	659±208	113±45	545.5±208	0.54±0.44	2.04±0.12
071010A	0.98	6	2.18±0.34	0.14±0.02	2.10±0.91	-2.00±0.15	61364±5918	17/16	82915±22557	30178±9884	52737±21935	0.42±0.42	3.59±0.22
080307	...	125.9	1.71±0.20	66.39±2.09	0.80±0.10	-2.00±0.03	270±7	209/157	377±22	179±12	198±21	1.04±0.05	3.43±0.04
080319C	1.95	34	1.55±0.10	70.32±4.20	1.85±0.46	-1.38±0.02	434±23	107/55	807±107	198±38	608±105	0.60±0.24	2.72±0.06
081028	3.038	260	1.94±0.07	0.89±0.28	1.53±0.12	-1.96±0.04	22951±559	1850/649	27151±1815	9882±882	17269±1772	0.69±0.05	3.47±0.05
090205	4.6497	8.8	1.95±0.15	0.94±0.08	0.98±0.32	-1.10±0.04	1000±123	135/34	2013±502	608±166	1405±505	1.12±0.18	2.21±0.08
090429B	9.3	5.5	1.87±0.22	2.13±0.17	1.57±0.34	-1.40±0.06	574±49	35/16	1066±211	262±71	804±211	0.74±0.17	2.71±0.09
101024A	...	18.7	1.77±0.12	10.27±0.83	0.60±0.17	-1.20±0.03	500±57	101/55	957±213	349±75	608±215	1.32±0.10	2.27±0.06
110213A	1.46	48	1.86±0.06	34.65±1.67	0.60±0.09	-1.50±0.01	1433±65	1054/245	2923±305	721±125	2202±294	1.25±0.05	2.70±0.03
110715A	0.82	13	1.82±0.19	0.84±0.06	2.07±0.53	-1.37±0.05	38689±2080	6388/253	62722±9968	9832±3610	52890±9746	0.48±0.27	2.74±0.09
120326A	1.798	69.6	1.85±0.07	1.21±0.03	1.00±0.07	-1.90±0.05	37336±983	2754/242	53073±3660	13063±1699	40009±3527	0.96±0.03	3.32±0.07
130511A	1.3033	5.43	1.85±0.17	5.71±0.68	1.40±0.83	-1.11±0.03	150±19	46/25	264±87	65±32	199±86	0.88±0.46	2.29±0.14
130831B	...	37.8	1.96±0.17	8.64±0.55	2.16±0.59	-1.03±0.03	455±33	104/42	1066±195	113±53	953±193	0.46±0.32	2.29±0.08
140515A	6.32	23.4	1.73±0.12	1.86±0.14	2.55±0.28	-1.38±0.04	2932±147	253/53	5088±795	797±236	4290±787	0.23±0.14	2.80±0.06
150103A	...	49.1	1.82±0.40	75.85±2.96	2.00±0.27	-2.53±0.07	220±6	98/65	199±18	49±10	150±17	0.43±0.11	4.29±0.10
150626B	...	48	2.02±0.15	1.09±0.05	0.96±0.10	-2.23±0.12	21828±962	313/79	30370±3486	7475±1670	22895±3349	0.93±0.05	3.77±0.16
150911A	...	7.2	1.96±0.14	6.65±0.40	1.64±0.12	-1.84±0.06	1905±76	1950/107	1857±273	456±142	1401±256	0.65±0.06	3.32±0.08
161001A	...	2.6	1.97±0.16	40.88±1.99	1.19±0.35	-1.07±0.01	109±7	196/79	199±29	49±11	151±29	1.01±0.19	2.20±0.06
171205A	0.0368	189.4	1.63±0.17	0.10±0.01	0.45±0.12	-1.06±0.05	58429±7174	7439/211	152975±33264	43367±8808	109608±33643	1.45±0.07	2.03±0.08
181110A	1.505	138.4	1.83±0.09	13.81±0.79	0.93±0.14	-1.79±0.05	1711±110	12832/264	2463±394	606±187	1857±380	1.02±0.07	3.16±0.08

NOTE—

^a In units of $10^{-11} \text{ erg cm}^{-2} \text{ s}^{-1}$.^b In units of seconds.

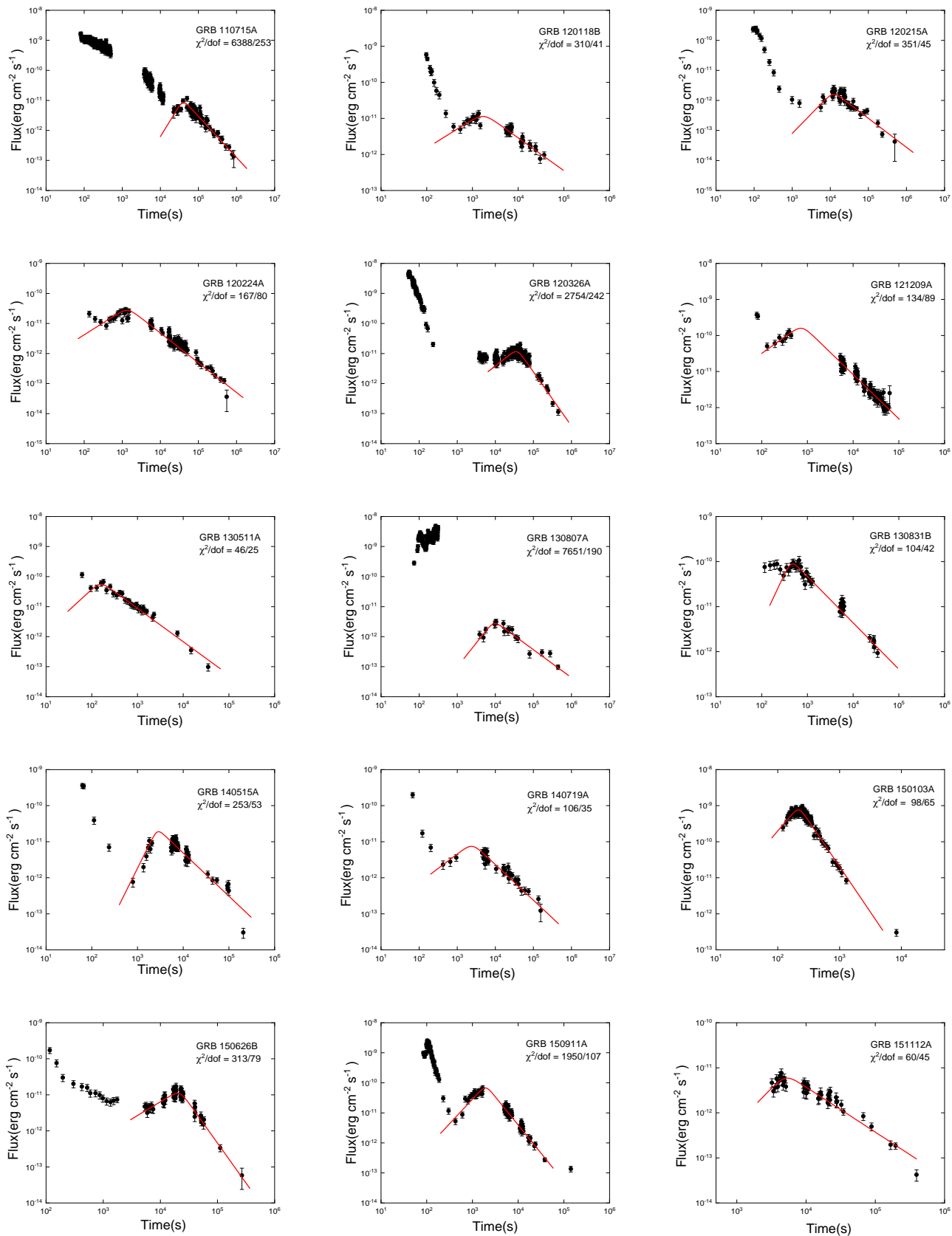


Figure 1 (Continued)

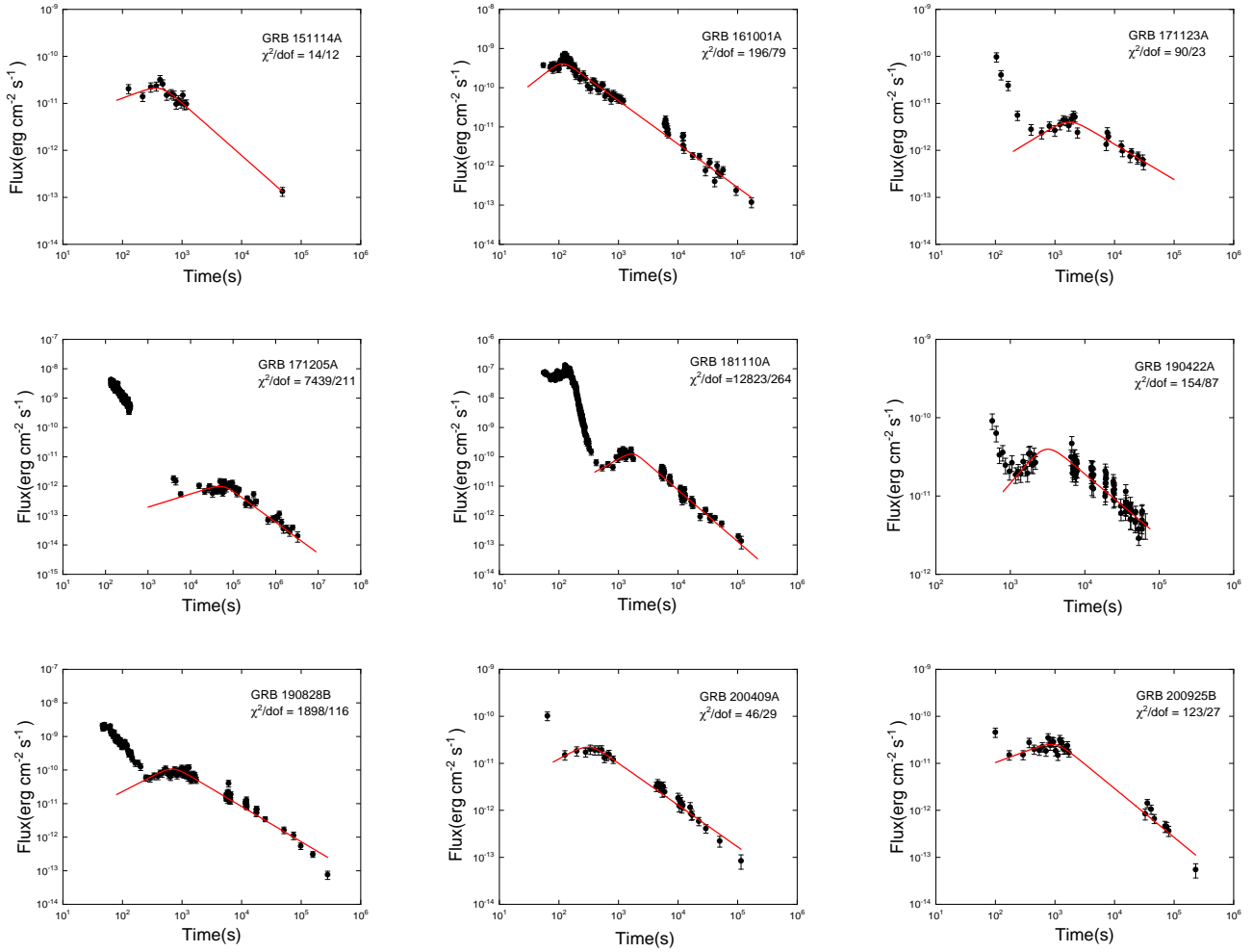


Figure 1 (Continued)

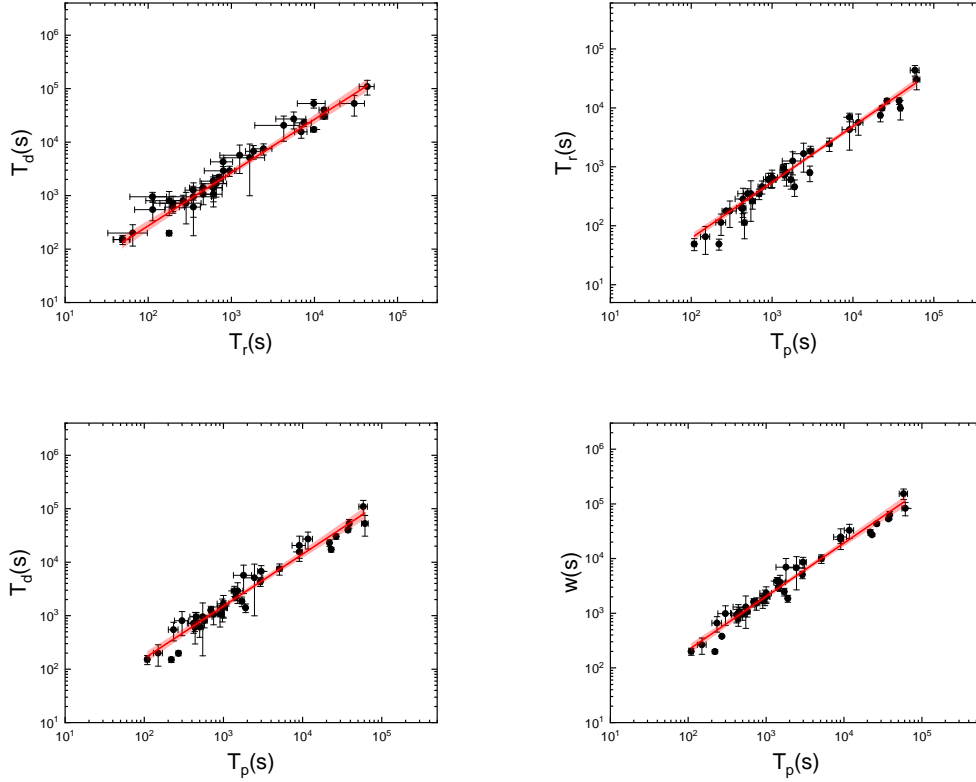


Figure 2. Pair correlations among the fitting parameters of the selected sample. Lines are the best fits.

tral index p are two factors in determining the slopes before and after the peak time of light curves. Here, we do not consider the regime of $\nu < \{\nu_c^f, \nu_m^f\}$, as it is very rare to show in X-ray band. In the following, we will take GRB 070103 and GRB 090429B as two typical examples to elaborate how the index k and p are determined.

4.1. GRB 070103

GRB 070103 was detected by *Swift*/BAT with a duration $T_{90} = 18.6$ s and thus belongs to a long GRB. Therefore, its circumburst medium is most likely to be a stellar wind environment, as long GRBs are widely believed to originate from the core collapse of massive stars. In the afterglow light curve, the flux increases with the time, i.e., $F_\nu \propto t^{0.55 \pm 0.16}$ before the peak time $T_p = 905 \pm 124$ s, and then decays after the peak, i.e., $F_\nu \propto t^{-1.32 \pm 0.05}$. We then consider both $\nu > \max\{\nu_c^f, \nu_m^f\}$ and $\nu_m^f < \nu < \nu_c^f$ regimes to determine the circumburst medium of GRB 070103.

(1) $\nu > \max\{\nu_c^f, \nu_m^f\}$. According to the Equations (6) and (7), we know that the temporal slopes of the onset bumps are determined by the medium density distribution index k and the electron spectral index p . We then have the decay index $\alpha_2 = (3p - 2)/4 = 1.32 \pm 0.05$, and thus the value of $p = 2.43 \pm 0.06$. Similarly, the rise index $\alpha_1 = (8 - 2k - kp)/4 = 0.55 \pm 0.16$, so

$k = (8 - 4\alpha_1)/(2 + p) = 1.31 \pm 0.14$. As we also have the expression $p = 2\beta_x = 2.20 \pm 0.54$, then the X-ray spectral index $\beta_x = 1.10 \pm 0.27$ in regime of $\nu > \max\{\nu_c^f, \nu_m^f\}$, which is consistent with the value calculated by the temporal slopes. In this case, the values k and p are both reasonable (generally supposed $0 < k < 2$ and $2 < p < 3$). We then apply the regime $\nu > \max\{\nu_c^f, \nu_m^f\}$ to infer the ambient medium of GRB 070103, and obtain $k = 1.31 \pm 0.14$ and $p = 2.43 \pm 0.06$, respectively.

(2) $\nu_m^f < \nu < \nu_c^f$. According to the theoretical analysis above, we obtain $\alpha_1 = (12 - 5k - kp)/4$ and $\alpha_2 = (12p - 3kp - 12 + 5k)/(16 - 4k)$, as well as $k = 1.32 \pm 0.09$ and $p = 2.43 \pm 0.07$ for the temporal slopes. In this case, $p = 2\beta_x + 1 = 3.20 \pm 0.54$, which is not consistent with that derived from the temporal indexes. As a result, this case $\nu_m^f < \nu < \nu_c^f$ may not be suitable to identify the type of the ambient medium for GRB 070103.

We conclude that the $\nu > \max\{\nu_c^f, \nu_m^f\}$ case might be used to explain the ambient medium of GRB 070103. We then obtain the medium density profile of the GRB 070103, i.e., $n \propto R^{-1.31}$. This indicates that the ambient medium of GRB 070103 is neither a homogeneous ISM for $k = 0$, nor the typical interstellar wind environment for $k = 2$. It indicates that the ambient medium of GRB 070103 may be in the intermediate regime, between ISM and the stellar wind.

4.2. GRB 090429B

The GRB 090429B has a duration $T_{90} = 5.5s$. In our study, we fit the afterglow by using an empirical smooth broken power-law function. Then we have the rise index $\alpha_1 = 1.57 \pm 0.34$, and the decay index $\alpha_2 = -1.40 \pm 0.06$. We also consider the two following regimes $\nu > \max\{\nu_c^f, \nu_m^f\}$ and $\nu_m^f < \nu < \nu_c^f$, respectively.

(1) $\nu > \max\{\nu_c^f, \nu_m^f\}$. In this case, we obtain $k = 0.38 \pm 0.29$ and $p = 2.53 \pm 0.07$ for rise-decay indices. Combining the theoretical spectral index, we obtain $p = 2\beta_x = 1.74 \pm 0.44$ with $\beta_x = 0.87 \pm 0.22$ for GRB 090429B. This result is inconsistent with the constraint of the temporal slopes. Therefore, the regime of $\nu > \max\{\nu_c^f, \nu_m^f\}$ may be not suitable for the X-ray light curve of GRB 090429B.

(2) $\nu_m^f < \nu < \nu_c^f$. In this case, $p = 2\beta_x + 1 = 2.74 \pm 0.44$. Combining with the rise-decay indices, we have the rise index $\alpha_1 = (12 - 5k - kp)/4$ and the decay index $\alpha_2 = (12p - 3kp - 12 + 5k)/(16 - 4k)$, respectively. We then obtain $k = 0.74 \pm 0.17$ and $p = 2.71 \pm 0.09$, respectively. Both $k = 0.74 \pm 0.17$ and $p = 2.71 \pm 0.09$ are in a reasonable range. Therefore, the $\nu_m^f < \nu < \nu_c^f$ case of the FS model can be used to explain the X-ray light curve of GRB 090429B. And we here adopt the values of $k = 0.74 \pm 0.17$ and $p = 2.71 \pm 0.09$ for GRB 090429B.

After applying the FS model with the uncertainty index k to the rest of X-ray samples, we find that the value k is centered at around 1.0, with a range of 0.2 and 1.8. Figure 3 shows the distribution of k and p features. The values of p is between 1.7 and 3.8. Our results indicate that the X-ray onset bumps could also be applied to constrain the circumburst medium of long GRBs, further implying that GRBs may have diverse ambient media.

5. DISCUSSIONS

The afterglows of GRBs are generally considered as efficient tools to probe the properties of the circumburst medium (Yi et al. 2013; Liang et al. 2013). Different authors have reached a consistent result, but with a slight deviation mainly due to the different sample selections. These works involve the constraints from the GRB 970616 (Dai & Lu 1998), from a subsample of ten *BeppoSAX* GRBs with the simultaneous spectra of X-ray, optical, and NIR afterglow data (Starling et al. 2008), from *Swift* GRBs with late-time optical and *Swift*/X-ray afterglow (Schulze et al. 2011), as well as from a subsample of GRB optical afterglows with onset bump features (Yi et al. 2013; Liang et al. 2013; Zhou et al. 2020). The results from these studies indicate that the circumburst medium of GRBs is not simply a wind environment, or an ISM.

From a theoretical point of view, The circumburst medium of GRBs, in general, is complex. It is accepted

that WR stars are the progenitors of long GRBs, however, the mass-loss rates of WR stars are still one of the major uncertainties in modern astrophysics (Sander & Vink 2020). These progenitor stars are expected to have significant stellar winds throughout the last stages of their evolution, which will thus play a key role in the conditions of the ambient environment. Information for the environment around the star after exploding, can be obtained with the observed properties of the afterglow. Two types are generally assumed, i.e., a wind environment ($k = 2$) and a homogeneous environment (ISM, $k = 0$). It is expected that the former case is favored based on our current understanding of stellar evolution. However, this is challenged by the observed properties of GBR afterglows.

6. CONCLUSIONS

In our extensive search for the onset bump characteristics in the early X-ray light curves, we have collected 39 GRBs, 20 of which have the redshift measurements. By applying the publicly-accepted empirical broken power-law function to fit the X-ray onset bumps, we derive the corresponding indices α_1 and α_2 for the temporal before and after the peak time T_p , as well as the peak flux time F_p . We find that the rise index α_1 for most GRBs falls in the range of 0.3–2.6, and that the central value of the decay index α_2 is around -1.0. Interestingly, we find that the characteristic time scales of the X-ray onset bumps have tight correlations, which are the same as those in the optical onset bumps.

In the standard collapsar model, the afterglow is believed to originate in the external shock produced as the blast wave collides with and sweeps up material in the ambient interstellar medium. In this work, by applying the external FS model to the onset bumps of X-ray light curves, we identify the circumburst medium of our target GRB samples. A systematic investigation of the temporal and spectral shows that the center value of the new inferred k is around 1.0, with a range from 0.2 to 1.8. This indicates that GRBs circumburst environment may be miscellaneous, neither the ISM nor the typical interstellar wind.

7. ACKNOWLEDGMENTS

We thank the anonymous referee for the helpful comments and suggestions. We also thank Yuan-Chuan Zou, Xue-Feng Wu, En-Wei Liang and Qing-Wen Tang for helpful discussions. This work was supported by the National Natural Science Foundation of China (Grant Nos. U2038106, U1931106), Ying Qin acknowledges the support from the Doctoral research start-up funding of Anhui Normal University and the funding from Key Laboratory for Relativistic Astrophysics in Guangxi University, Shandong Provincial Natural Science Foundation of

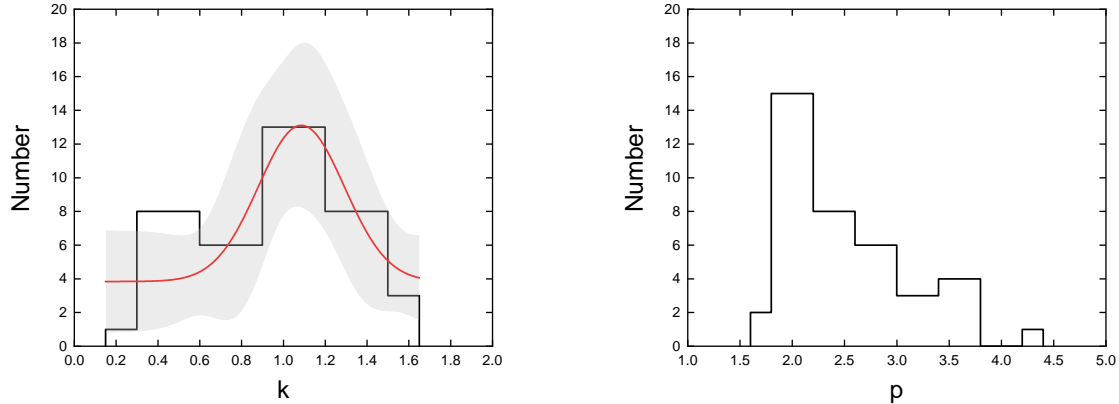


Figure 3. Distributions of the values k and p of our sample. The red line is the Gauss fitting line with 1σ error bars.

China(grant No. ZR2019YQ03).

REFERENCES

- Atwood, W. B., Abdo, A. A., Ackermann, M., et al. 2009, *ApJ*, 697, 1071. doi:10.1088/0004-637X/697/2/1071
- Beuermann, K., Hessman, F. V., Reinsch, K., et al. 1999, *A&A*, 352, L26
- Burrows, D. N., Hill, J. E., Nousek, J. A., et al. 2005, *Space Sci. Rev.*, 120, 165. doi:10.1007/s11214-005-5097-2
- Cantiello, M., Yoon, S.-C., Langer, N., et al. 2007, *A&A*, 465, L29. doi:10.1051/0004-6361:20077115
- Dai, Z. G. & Lu, T. 1998, *MNRAS*, 298, 87. doi:10.1046/j.1365-8711.1998.01681.x
- Du, M., Yi, S.-X., Liu, T., et al. 2021, *ApJ*, 908, 242. doi:10.3847/1538-4357/abd6bd
- Detmers, R. G., Langer, N., Podsiadlowski, P., et al. 2008, *A&A*, 484, 831. doi:10.1051/0004-6361:200809371
- Gehrels, N., Chincarini, G., Giommi, P., et al. 2004, *ApJ*, 611, 1005. doi:10.1086/422091
- Ghirlanda, G., Nava, L., Ghisellini, G., et al. 2012, *MNRAS*, 420, 483. doi:10.1111/j.1365-2966.2011.20053.x
- Japelj, J., Kopač, D., Kobayashi, S., et al. 2014, *ApJ*, 785, 84. doi:10.1088/0004-637X/785/2/84
- Li, L., Wang, X.-G., Zheng, W., et al. 2020, *ApJ*, 900, 176. doi:10.3847/1538-4357/aba757
- Li, Y., Wen, X., Sun, X., et al. 2020, *Scientia Sinica Physica, Mechanica & Astronomica*, 50, 129508. doi:10.1360/SSPMA-2019-0417
- Liang, E.-W., Li, L., Gao, H., et al. 2013, *ApJ*, 774, 13. doi:10.1088/0004-637X/774/1/13
- Liang, E.-W., Yi, S.-X., Zhang, J., et al. 2010, *ApJ*, 725, 2209. doi:10.1088/0004-637X/725/2/2209
- Liu, T., Gu, W.-M., & Zhang, B. 2017, *New A Rev.*, 79, 1. doi:10.1016/j.newar.2017.07.001
- Liu, T., Song, C.-Y., Zhang, B., et al. 2018, *ApJ*, 852, 20. doi:10.3847/1538-4357/aa9e4f
- MacFadyen, A. I. & Woosley, S. E. 1999, *ApJ*, 524, 262. doi:10.1086/307790
- Meegan, C., Lichti, G., Bhat, P. N., et al. 2009, *ApJ*, 702, 791. doi:10.1088/0004-637X/702/1/791
- Mészáros, P. & Rees, M. J. 1993, *ApJ*, 405, 278. doi:10.1086/172360
- Mészáros, P. & Rees, M. J. 1997, *ApJ*, 476, 232. doi:10.1086/303625
- Mészáros, P. 2002, *ARA&A*, 40, 137. doi:10.1146/annurev.astro.40.060401.093821
- Molinari, E., Vergani, S. D., Malesani, D., et al. 2007, *A&A*, 469, L13. doi:10.1051/0004-6361:20077388
- Nousek, J. A., Kouveliotou, C., Grupe, D., et al. 2006, *ApJ*, 642, 389. doi:10.1086/500724
- Oates, S. R., Page, M. J., Schady, P., et al. 2009, *MNRAS*, 395, 490. doi:10.1111/j.1365-2966.2009.14544.x
- Panaiteescu, A. & Kumar, P. 2002, *ApJ*, 571, 779. doi:10.1086/340094
- Piran, T. 2004, *Reviews of Modern Physics*, 76, 1143. doi:10.1103/RevModPhys.76.1143
- Qin, Y., Liang, E.-W., Liang, Y.-F., et al. 2013, *ApJ*, 763, 15. doi:10.1088/0004-637X/763/1/15
- Qin, Y., Fragos, T., Meynet, G., et al. 2018, *A&A*, 616, A28. doi:10.1051/0004-6361/201832839
- Rees, M. J. & Meszaros, P. 1994, *ApJL*, 430, L93. doi:10.1086/187446
- Roming, P. W. A., Kennedy, T. E., Mason, K. O., et al. 2005, *Space Sci. Rev.*, 120, 95. doi:10.1007/s11214-005-5095-4
- Rykoff, E. S., Aharonian, F., Akerlof, C. W., et al. 2009, *ApJ*, 702, 489. doi:10.1088/0004-637X/702/1/489
- Sari, R. & Piran, T. 1999, *ApJ*, 520, 641. doi:10.1086/307508
- Sari, R., Piran, T., & Narayan, R. 1998, *ApJL*, 497, L17. doi:10.1086/311269
- Si, S.-K., Qi, Y.-Q., Xue, F.-X., et al. 2018, *ApJ*, 863, 50. doi:10.3847/1538-4357/aad08a
- Schulze, S., Klose, S., Björnsson, G., et al. 2011, *A&A*, 526, A23. doi:10.1051/0004-6361/201015581
- Starling, R. L. C., van der Horst, A. J., Rol, E., et al. 2008, *ApJ*, 672, 433. doi:10.1086/521975
- Sander, A. A. C. & Vink, J. S. 2020, *MNRAS*, 499, 873. doi:10.1093/mnras/staa2712
- Wang, X.-G., Zhang, B., Liang, E.-W., et al. 2018, *ApJ*, 859, 160. doi:10.3847/1538-4357/aabc13
- Wang, F., Zou, Y.-C., Liu, F., et al. 2020, *ApJ*, 893, 77. doi:10.3847/1538-4357/ab0a86
- Woosley, S. E. 1993, *ApJ*, 405, 273. doi:10.1086/172359
- Yi, S.-X., Wu, X.-F., Zou, Y.-C., et al. 2020, *ApJ*, 895, 94. doi:10.3847/1538-4357/ab8a53
- Yi, S.-X., Xi, S.-Q., Yu, H., et al. 2016, *ApJS*, 224, 20. doi:10.3847/0067-0049/224/2/20
- Yi, S.-X., Wu, X.-F., & Dai, Z.-G. 2013, *ApJ*, 776, 120. doi:10.1088/0004-637X/776/2/120
- Yi, S.-X., Xie, W., Ma, S.-B., et al. 2021, *MNRAS*, 507, 1047. doi:10.1093/mnras/stab2186

- Yi, S.-X., Lei, W.-H., Zhang, B., et al. 2017, *Journal of High Energy Astrophysics*, 13, 1. doi:10.1016/j.jheap.2017.01.001
- Yi, S.-X., Du, M., & Liu, T. 2021, arXiv:2111.01041
- Zhang, B. & Mészáros, P. 2004, *International Journal of Modern Physics A*, 19, 2385. doi:10.1142/S0217751X0401746X
- Zhang, B., Fan, Y. Z., Dyks, J., et al. 2006, *ApJ*, 642, 354. doi:10.1086/500723
- Zhang, S.-N., Li, T., Lu, F., et al. 2020, *Science China Physics, Mechanics, and Astronomy*, 63, 249502. doi:10.1007/s11433-019-1432-6
- Zhao, W., Zhang, J.-C., Zhang, Q.-X., et al. 2020, *ApJ*, 900, 112. doi:10.3847/1538-4357/aba43a
- Zhou, Q.-Q., Yi, S.-X., Huang, X.-L., et al. 2020, *International Journal of Modern Physics D*, 29, 2050043. doi:10.1142/S0218271820500431